Imaging nanoparticles in cells by nanomechanical holography

LAURENE TETARD[1,2], ALI PASSIAN[1,2]*, KATHERINE T. VENMAR[1], RACHEL M. LYNCH[1], BRYNN H. VOY[1], GAJENDRA SHEKHAWAT[3], VINAYAK P. DRAVID[3] AND THOMAS THUNDAT[1,2]

[1]Biosciences Division, Oak Ridge National Laboratory, Oak Ridge, Tennessee 37831, USA
[2]Department of Physics, University of Tennessee, Knoxville, Tennessee 37996-1200, USA
[3]Materials Science & Engineering department, Northwestern University, Evanston, Illinois 60208, USA
*e-mail: passianan@ornl.gov

Published online: 22 June 2008; doi:10.1038/nnano.2008.162

Nanomaterials have potential medical applications, for example in the area of drug delivery, and their possible adverse effects and cytotoxicity are curently receiving attention[1,2]. Inhalation of nanoparticles is of great concern, because nanoparticles can be easily aerosolized. Imaging techniques that can visualize local populations of nanoparticles at nanometre resolution within the structures of cells are therefore important[3]. Here we show that cells obtained from mice exposed to single-walled carbon nanohorns can be probed using a scanning probe microscopy technique called scanning near field ultrasonic holography. The nanohorns were observed inside the cells, and this was further confirmed using micro Raman spectroscopy. Scanning near field ultrasonic holography is a useful technique for probing the interactions of engineered nanomaterials in biological systems, which will greatly benefit areas in drug delivery and nanotoxicology.

The rising commercial use and large-scale production of engineered nanoparticles may lead to unintended exposure in humans[1–4]. Studies have suggested that the toxicity of nanoparticles varies widely according to the chemical and physical characteristics of the particle[5,6], so particle-specific toxicity studies are urgently needed[7,8]. To date, electron microscopy has been the most common technique used to study intracellular structures[9,10]. An analytical technique that can examine a surrogate, minimally invasive test system such as blood or fluid that has been washed out from the lungs (known as bronchoalveolar lavage, BAL) will be a useful screening tool.

Transmission electron microscopy (TEM) can only identify aggregates of nanotubes within alveolar macrophages[10,11]. Very recently, carbon nanotubes were observed inside lysosomes using TEM[11]. For a comparable resolution, atomic force microscopy (AFM) has the advantages[12–16] of easier sample preparation and the possibility of ambient imaging. However, conventional AFM using a cantilever tip can only probe the surface of a specimen, making it difficult to analyse structures that are inside a cell. This limitation arises from there being insufficient mechanical excitation of the sample, resulting in the inability of the probe to gather information on the subsurface properties.

The recently developed technique known as scanning near field ultrasonic holography (SNFUH)[17] (see Supplementary Information) offers a way to image soft samples and probe structures that are below their surfaces. If a cell is oscillated at

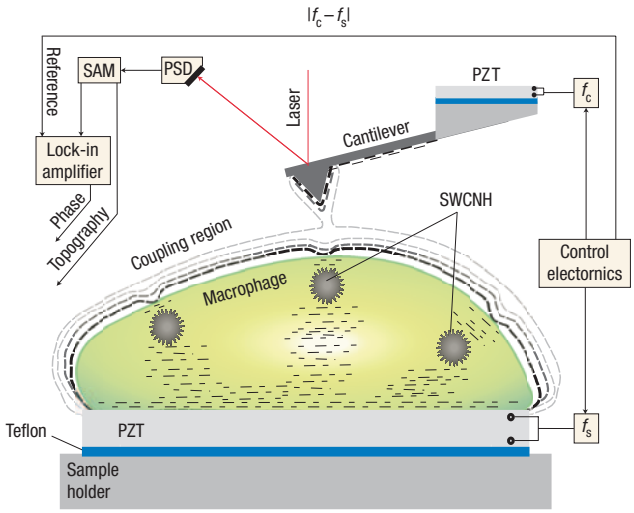

Figure 1 Intracellular imaging of aspirated nanoparticles using ultrasonic holography. The signal access module (SAM) provides the instantaneous location of the reflected laser beam as monitored by a position-sensitive detector (PSD). The dynamics of the cantilever is presented at the input of a lock-in amplifier. The local perturbation in the coupled oscillations of the ultrasonic-driven microcantilever–macrophage system is monitored with the lock-in using the difference frequency $f_c - f_s$ as reference. By mapping the strength of the coupling in a scanned area of the cell, a phase image emerges that contains information on the buried SWCNHs.

megahertz frequencies f_s using a piezoelectric crystal, the ultrasonic waves travelling through the oscillating cell structure may weakly drive an AFM cantilever that is in contact with the cell surface, as long as the elastic properties of the cell can support a propogation mode in the ultrasonic spectrum (Fig. 1). If the cantilever is independently vibrated at a slightly different frequency f_c, then the nonlinear tip–surface interaction may result in a measurable coupling. The detection of this local coupling between the two oscillators may be used to probe the subsurface cellular information. The phase information in the coupled mode may be detected using the difference frequency as

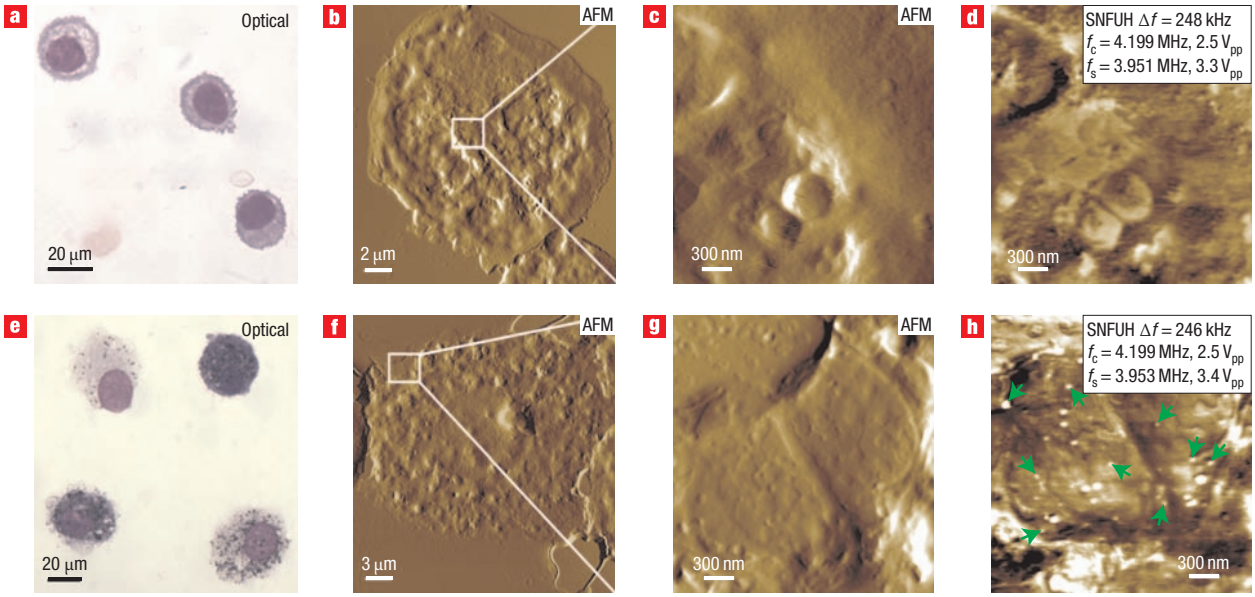

Figure 2 Presence of SWCNHs inside cells obtained from mice lungs. a–h, Alveolar macrophages from vehicle control (**a–d**) and mice exposed to SWCNH after 7 days (**e–h**). Representative optical (**a**,**e**), AFM topography (**b**,**c**,**f**,**g**) and SNFUH (**d**,**h**) images from control and treated mice. White dots in **h** (some indicated by green arrows) correspond to SWCNHs.

reference for the lock-in which can be displayed as a function of the spatial location of the scanning cantilever tip. (Similar interactions have recently been investigated in a mathematical model[18].) The resultant phase map may reveal any contrasts due to acoustic impedance variation, which results from nanoscale heterogeneity in the volume of the cell directly under the AFM tip, and effectively constitutes a mapping of the cell's elastic response. The ability to acquire simultaneous topography and holography information with nanometre image resolution suggests that SNFUH could be a potential method to probe cellular uptake of nanoparticles. We explored this viability to determine the cellular fate of single-walled carbon nanohorns (SWCNHs) using a

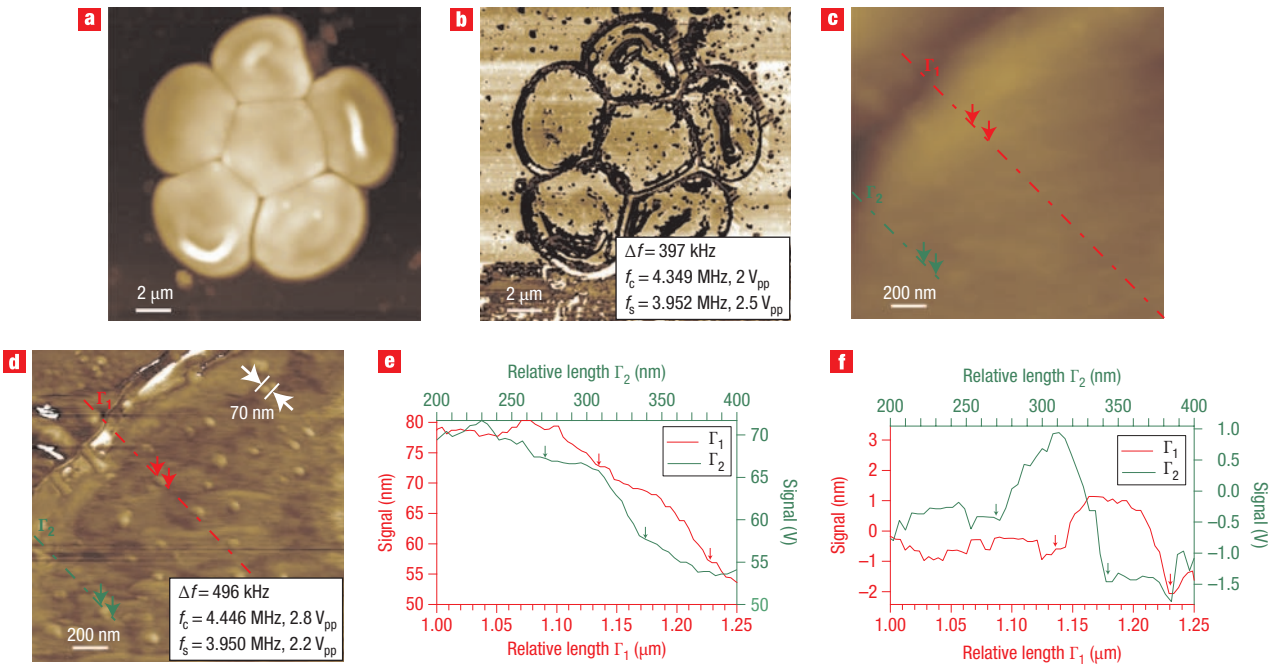

Figure 3 Nanoparticles detected inside red blood cells. a–d, AFM topography (**a**,**c**) and SNFUH phase (**b**,**d**) images of erythrocytes obtained from the BAL fluid of an SWCNH-exposed mouse 24 h post-aspiration. **e**,**f**, Profiles taken along Γ_1 and Γ_2 across nanohorns buried in **c** and **d**, respectively, show that SNFUH can resolve nanoparticles that are inside the cells.

mouse model to detect and visualize particles within lavage cells and blood.

Optical images of macrophages collected from both vehicle controls (untreated) and SWCNH-treated mice killed 7 days after exposure (Fig. 2) reveal the presence of variously sized carbonaceous aggregates within the cytoplasm of macrophages from SWCNH-exposed mice (Fig. 2e) that are not present in controls (Fig. 2a) or in erythrocytes. The region occupied by the nucleus is readily detected and the characteristic macrophage morphology is present in both samples (Fig. 2b,f). The topographic image of an alveolar macrophage from an SWCNH-exposed mouse reveals nanoparticles on the surface of the cell (Fig. 2g).

A striking visualization of the nanohorns was obtained from the SNFUH image of the same macrophage (Fig. 2h), revealing several SWCNHs within the cell (marked with arrows in Fig. 2h), which are not visible in Fig. 2d,g. The sizes of these particles are statistically consistent with the size distribution (70–110 nm) established from analysing several AFM images of the SWCNH solution, indicating that nanoparticles, rather than larger aggregates, were taken up by the macrophages. The contrast measures the phase of the local tip–cell surface coupling, and originates from the difference in elasticity and density between the SWCNH and the cell.

Interestingly, as in the case of macrophages from SWCNH-exposed mice, we encounter nanoparticles within erythrocytes that were present (although rare) in BAL samples (see Methods). Figure 3a,b shows the topography and SNFUH phase images of erythrocytes that were present in BAL fluid extracted from a mouse 24 h after SWCNH exposure. Although the topography image only resolves nanoparticles on the cellular surface of the erythrocytes (Fig. 3a), a surprisingly large number of additional particles are detected in the SNFUH image captured at the same location (Fig. 3b). Higher resolution images of the topography (Fig. 3c) and the SNFUH image (Fig. 3d) consistently compare well and show particles with an average diameter of 70–110 nm, as is reinforced in Fig. 3e,f (see Methods). The profiles in Fig. 3e,f were taken along the lines Γ1 and Γ2 across buried nanohorns in Fig. 3c,d to help establish that no nanoparticles were located on the top surface of the cell, as seen in Fig. 3e where no nanoparticle-like features can be observed in contrast to Fig. 3f.

To determine if SWCNH association with erythrocytes was due to systemic translocation[19], we used SNFUH to image peripheral blood samples. The results for peripheral blood from a control mouse obtained using AFM and SNFUH are depicted in Fig. 4a,b, respectively. The images from an exposed mouse (AFM and SNFUH, Fig. 4c,d, respectively) show contrast areas with sizes matching those of the nanohorns. This observation is supported by further images in Fig. 4e–j. Note that the difference in contrast between images in Fig. 2h and 3d (appearing in white) and Fig. 4j (appearing in black) is due to a difference in the phase accretion associated with the coupling between the oscillations of the cantilever and the cell as shown schematically by the contours in Fig. 1.

The SNFUH images in Fig. 4 presenting an intracellular SWCNH population in the peripheral blood from exposed mice support earlier published results[9], in which nano-sized polystyrene beads were observed to be taken up by erythrocytes *in vitro*.

As control, the measurements were repeated using silica nanoparticles. Similarly, topographic and SNFUH images reveal the presence of silica within the cell, confirming the ability of SNFUH to resolve the presence of materials of different stiffness (see Supplementary Information, Fig. S1).

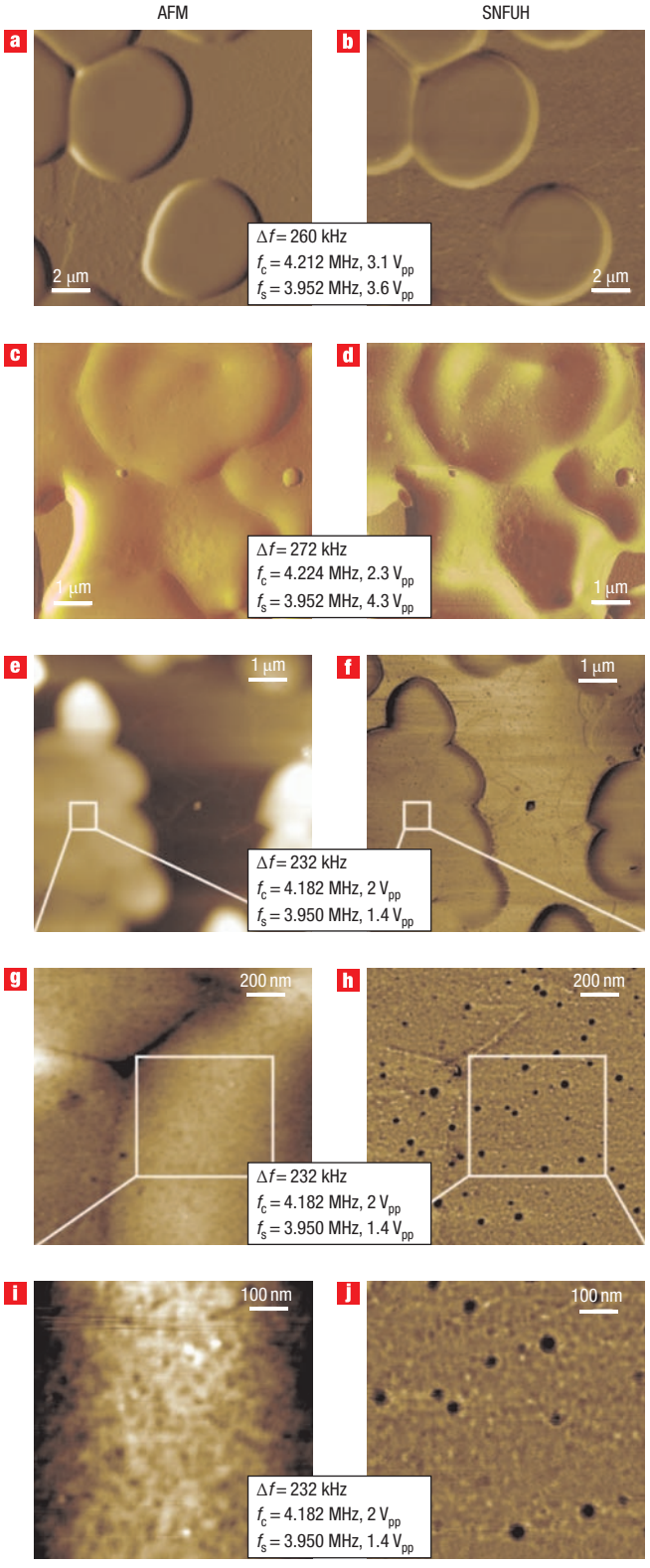

Figure 4 High-resolution images of nanoparticles in red blood cells. **a**–**j**, AFM topography (left panels) and SNFUH phase images (right panels) of erythrocytes obtained from a control mouse (**a**,**b**) and a SWCNH-exposed mouse sacrificed 24 h after exposure (**c**–**j**). Successive reduction in scan size (24.4 μm to 3 μm to 1.55 μm) of the SNFUH images resolves the 80–100 nm particles inside the cells.

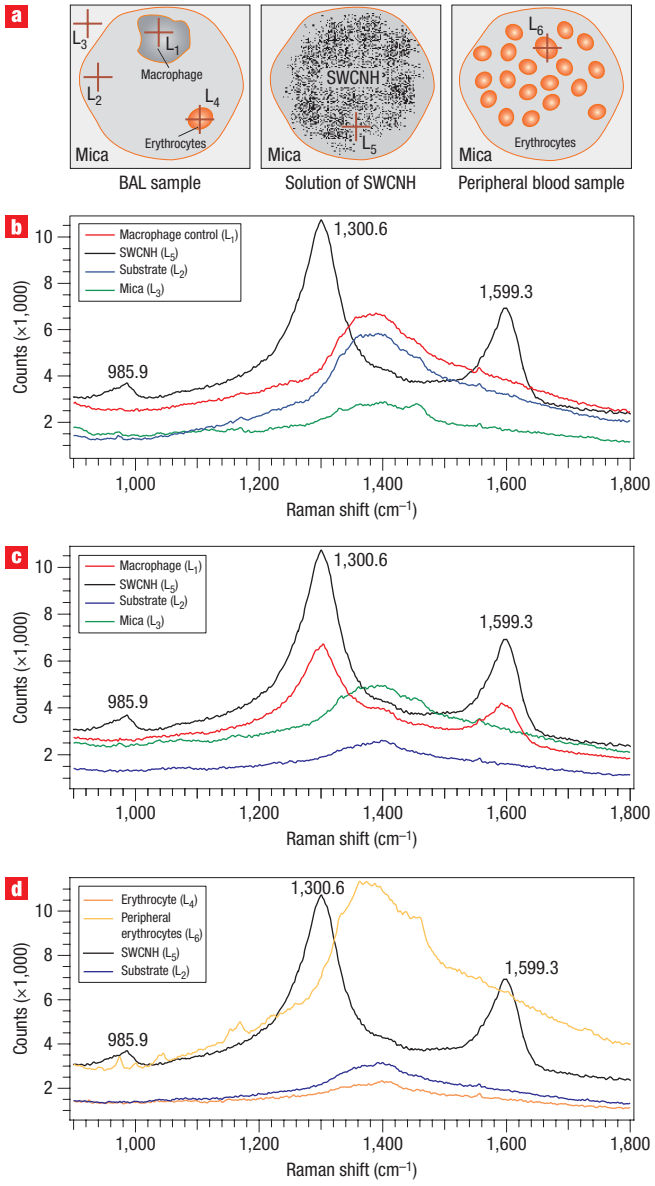

Figure 5 Confirming the presence of SWCNHs inside cells using Raman spectroscopy. a, Schematics showing the locations where Raman photons were collected from a treated BAL sample (left), a solution of SWCNHs used for aspiration (middle), and peripheral blood from treated mice (right). **b**,**c**, Raman spectra of vehicle control (**b**, untreated mice) and BAL sample 7 d after exposure (**c**). Measurements were taken within the macrophage (L_1, red), within the buffer (L_2, blue) and on the mica substrate (L_3, green). **d**, Raman spectra taken on erythrocytes in BAL samples (L_4, orange) and peripheral blood (L_6, yellow) do not show any signal for SWCNHs.

In order to further validate our results, that is, the detection of SWCNHs within the cellular structure, we carried out Raman spectroscopy of the macrophages (see Supplementary Information). For a threshold number density of buried nanohorns, we would expect to observe a sufficient Raman yield. As shown in Fig. 5, apart from substrate effects, the Raman spectrum of the SWCNH exhibits a minor band at 985.9 cm^{-1} and two major bands peaking at $k_D = 1{,}300.6\ cm^{-1}$ and $k_G = 1{,}599.3\ cm^{-1}$ (ref. 20) (black curve in Fig. 5). The results capture the Raman signatures of both the BAL samples from the vehicle control (Fig. 5b) and the exposed mice (Fig. 5c). Figure 5a presents the locations at which spectra were obtained (L_i). No traces of SWCNHs could be found for the case of control macrophages (Fig. 5b), whereas in the case of the exposed mouse strong evidence of SWCNHs can readily be identified (Fig. 5c) from the D and G bands[21,22]. No SWCNH bands could be detected in regions exterior to the macrophages, as shown in the measurements at points L_2 and L_3. Owing to the lower number densities of the SWCNHs in the erythrocytes, no Raman shift could be measured in the regions occupied by the cells from both the BAL sample (L_4) and the peripheral blood (L_6) extracted from the mice (Fig. 5d).

The net effect of nanoparticle exposure on health[3,4] is an area of active research and controversy. Understanding the fate of nanoparticles within the body is critical to assessing both their potential toxicity[23–25] and their efficacy in realizing their potential as vehicles of drug delivery[26]. We have demonstrated that SNFUH offers a means to monitor the cellular deposition of nanoparticles following *in vivo* exposure.

To summarize, the results show the presence of SWCNHs within macrophages of mouse aspirated with nanoparticles. We visualized nanoparticles within both alveolar macrophages and peripheral erythrocytes. Raman spectroscopy carried out on macrophages supports our conclusion of the presence of SWCNHs within the cells. The subsurface imaging capability of SNFUH will help advance the field of nanoparticle–cell interactions. The important advantages of this method include high-resolution subsurface imaging and localization of nanoparticles in biological samples, its compatibility with ambient conditions, minimal sample preparation, and the fact that it does not require any labelling to be carried out. Moreover, compared to techniques such as TEM, SNFUH offers relatively high-throughput sample analysis, enabling the imaging of a population of cells within a reasonable timeframe. The SNFUH method should be particularly useful for determining the efficacy of cell-type-specific drug targeting, which is a critical goal in the development of medical uses of nanomaterials. Morphological parameters of cells can be used to distinguish cell types within a sample, providing the ability to assess cell-type-specific particle uptake without the need for labelling, as is required by many other imaging techniques. This method could also be useful in screening for nanoparticle exposure risk using peripheral blood. It is expected that our results will prove useful in resolving critical questions about the fate and potential toxicity of nanoparticles within the body.

METHODS

SINGLE-WALLED CARBON NANOHORNS

Belonging to the fullerene group of carbon allotropes, the recently discovered dahlia-like SWCNHs are particularly attractive as potential intracellular delivery vehicles[20]. In our investigations, SWCNHs were produced in a high-temperature laser ablation system using a Nd:YAG laser (600 W maximum average power). Because SWCNHs are not soluble in phosphate buffered saline (PBS), the nonionic surfactant pluronic acid F-127 (Molecular Probes) was added to suspend the particles. Thus the aggregation tendency of the SWCNHs was attenuated. A 1 $\mu g\ \mu l^{-1}$ solution of SWCNHs was soluble in PBS with 1% pluronic. Pluronic-coated SWCNHs (diluted to 0.1 $\mu g\ \mu l^{-1}$ in PBS with 1% pluronic) alone were imaged with an AFM in contact mode in order to acquire topographic information for recognition purposes in BAL samples. Nanohorns were imaged using AFM by placing a vigorously vortexed drop on freshly cleaved mica, followed by air drying and then imaging. As a control, 1% pluronic in PBS was also analysed. All mica substrates were treated with a 1.2% solution of MgCl in order to neutralize the negative charge before adding the samples. The solution of SWCNHs suspended in PBS and pluronic was used to acquire the Raman spectra.

It was found that the carbon nanohorns assemble into spheres approximately 100 nm in diameter, which is consistent with previous studies that reported spherical masses with individual nanohorn projections around the

periphery, creating a dahlia-like structure[20]. In our experiments, the measured sizes agree well with those obtained from electron microscopy of nanohorns[20,27].

ANIMALS AND EXPERIMENTAL DESIGN

Each mouse was exposed to 30 μg of SWCNHs, an amount estimated to approximate OSHA-permissible exposure limits for graphite particles across twenty 8-h work days[24]. Agglomeration of the SWCNHs within the aspiration media (PBS) was controlled using the non-ionic surfactant pluronic F-127 and sonicating the solution before dosing, allowing the uptake of nanoparticles to be evaluated rather than larger agglomerates. Control and SWCNH-exposed mice were sacrificed 24 h and 7 d post-exposure.

Adult male mice from the stocks maintained at Oak Ridge National Laboratory (ORNL) were used in the study. All mice were housed in the specific pathogen-free facility at ORNL and given water and standard rodent chow *ad libitum*. The Animal Care and Use Committee at ORNL approved all experimental procedures. The mice were randomly assigned to two experimental groups: (1) the 1% pluronic/PBS aspiration group and (2) the 1 μg μl^{-1} SWCNHs in 1% pluronic/PBS aspiration group. Before exposure, the SWCNH solution was sonicated to ensure dispersion of the particles. Three mice from each group were sacrificed 24 h and 7 d after aspiration. Mouse pharyngeal aspiration was used for carbon nanohorn administration. Aspiration has been shown to consistently deliver particles to the alveolar region of the lung[28]. Aspiration was chosen because it is less traumatic and invasive than instillation, and is technically easier than inhalation. Aspiration was performed as previously described[24]. Briefly, mice were anaesthetized with isoflurane and hung by their incisors on an inclined board. The animal's tongue was extended using forceps, and 30 μl of the control solution or SWCNH solution was placed on the back of the tongue. The tongue was extended until all of the fluid was aspirated into the lungs.

SAMPLE PREPARATION

Mice were sacrificed by isoflurane overdose in a bell jar, and BAL was performed according to standard protocols. Briefly, the trachea was exposed and a blunt 22-gauge needle inserted into the trachea. After securing the needle with sutures, lavage was performed five times with cold sterile PBS. Fluid was gently aspirated while massaging the chest. The first lavage was performed with 0.6 ml of PBS and was kept separate for analysis for another study. The second and third lavages were performed with 1.0 ml of PBS and were pooled in sterile tubes, centrifuged, and resuspended in PBS. Soft tissue damage that may occur during the process of harvesting the BAL sample and/or cross-contamination of BAL fluid with blood as it is withdrawn from the lung can result in the rare observation of erythrocytes in the lavage. For light microscopy analysis, cytospin slides were stained with a Hema3 kit (Fisher Scientific). For AFM analysis, cells were centrifuged onto freshly cleaved mica using a cytospin and fixed with methanol. In addition, peripheral blood was collected using heparinized capillaries from the abdominal aorta. Blood samples were diluted in PBS, centrifuged onto freshly cleaved mica using a cytospin, and fixed with methanol.

Received 10 March 2008; accepted 13 May 2008; published 22 June 2008.

References

1. Nel, A., Xia, T., Madler, L. & Li, N. Toxic potential of materials at the nanolevel. *Science* **311,** 622–627 (2006).
2. Panessa-Warren, B. J., Warren, J. B., Wong, S. S. & Misewich, J. A. Biological cellular response to carbon nanoparticle toxicity. *J. Phys. Condens. Matter* **18,** S2185–S2201 (2006).
3. Stone, V. & Donaldson, K. Signs of stress. *Nature Nanotech.* **1,** 23–24 (2006).
4. Colvin, V. L. The potential environmental impact of engineered nanomaterials. *Nature Biotechnol.* **21,** 1166–1170 (2003).
5. Borm, P. *et al.* The potential risks of nanomaterials : a review carried out for ECETOC. *Part. Fibre Toxicol.* **3,** 11–46 (2006).
6. Xia, T. *et al.* Comparison of the abilities of ambient and manufactured nanoparticles to induce cellular toxicity according to an oxidative stress paradigm. *Nano Lett.* **6,** 1794–1807 (2006).
7. Oberdörster, G., Oberdörster, E. & Oberdörster, J. Nanotoxicology: an emerging discipline evolving from studies of ultrafine particles. *Environ. Health Perspect.* **113,** 823–839 (2005).
8. Holsapple, M. P. *et al.* Research strategies for safety evaluation of nanomaterials, Part II : Toxicological and safety evaluation of nanomaterials, current challenges and data needs. *Toxicol. Sci.* **88,** 12–17 (2005).
9. Geiser, M. *et al.* Ultrafine particles cross cellular membranes by nonphagocytic mechanisms in lungs and in cultured cells. *Environ. Health Perspect.* **113,** 1555–1560 (2005).
10. Wörle-Knirsch, J. M., Pulskamp, K. & Krug, H. F. Oops they did it again! Carbon nanotubes hoax scientists in viability assays. *Nano Lett.* **6,** 1261–1268 (2006).
11. Porter, A. E. *et al.* Direct imaging of single-walled carbon nanotubes in cells. *Nature Nanotech.* **2,** 713–717 (2007).
12. Rabe, U. & Arnold, W. Acoustic microscopy by atomic force microscopy. *Appl. Phys. Lett.* **64,** 1493–1495 (1994).
13. Kolosov, O. V. *et al.* Imaging the elastic nanostructure of Ge islands by ultrasonic force microscopy. *Phys. Rev. Lett.* **81,** 1046–1049 (1998).
14. Martinez, N. F., Patil, S., Lozano, J. R. & Garcia, R. Enhanced compositional sensitivity in atomic force microscopy by the excitation of the first two flexural modes. *Appl. Phys. Lett.* **89,** 153115 (2006).
15. Sahin, O. *et al.* An atomic force microscope tip designed to measure time-varying nanomechanical forces. *Nature Nanotech.* **2,** 507–514 (2007).
16. Garcia, R., Margerle, R. & Perez, R. Nanoscale compositional mapping with gentle forces. *Nature Mater.* **6,** 405–411 (2007).
17. Shekhawat, G. S. & Dravid, V. P. Nanoscale imaging of buried structures via scanning near-field ultrasound holography. *Science* **310,** 89–92 (2005).
18. Cantrell, S. A., Cantrell, J. H. & Lillehei, P. T. Nanoscale subsurface imaging via resonant different-frequency atomic force ultrasonic microscopy. *J. Appl. Phys.* **101,** 114324 (2007).
19. Kreyling, W. G., Semmler-Behnke, M. & Moller, W. Health implications of nanoparticles. *J. Nanopart. Res.* **8,** 543–562 (2006).
20. Iijima, S. *et al.* Nano-aggregates of single-walled graphitic carbon nano-horns. *Chem. Phys. Lett.* **309,** 165–170 (1999).
21. Tuinstra, F. & Koenig, J. L. Raman spectrum of graphite. *J. Chem. Phys.* **53,** 1126–1130 (1970).
22. Mathews, M. J., Pimenta, M. A., Dresselhaus, G., Dresselhaus, M. S. & Endo, M. Origins of dispersive effects of the Raman D band in carbon materials. *Phys. Rev. B* **59,** R6585–R6588 (1999).
23. Donaldson, K. *et al.* Carbon nanotubes: a review of their properties in relation to pulmonary toxicology workplace safety. *Toxicol. Sci.* **92,** 5–22 (2006).
24. Shvedova, A. A. *et al.* Unusual inflammatory and fibrogenic pulmonary responses to single-walled carbon nanotubes in mice. *Am. J. Physiol. Lung Cell Mol. Physiol.* **289,** L698–L708 (2005).
25. Lam, C.-W., James, J. T., McCluskey, R. & Hunter, R. L. Pulmonary toxicity of single-wall carbon nanotubes in mice 7 and 90 days after intratracheal instillation. *Toxicol. Sci.* **77,** 126–134 (2004).
26. Medina, C., Santos-Martinez, M. J., Radomski, A., Corrigan, O. I. & Radomski, M. W. Nanoparticles: pharmacological and toxicological significance. *Br. J. Pharmacol.* **150,** 552–558 (2007).
27. Fan, X., Tan, J., Zhang, G. & Zhang, F. Isolation of carbon nanohorn assemblies and their potential for intracellular delivery. *Nanotechnology* **18,** 195103 (2007).
28. Rao, G. V. *et al.* Efficacity of a technique for exposing the mouse lung to particles aspirated from the pharynx. *J. Toxicol. Environ. Health A* **66,** 1441–1452 (2003).

Supplementary Information accompanies this paper at www.nature.com/naturenanotechnology.

Acknowledgements

This research was sponsored in part by the ORNL BioEnergy Science Center. The BioEnergy Science Center is a U.S. Department of Energy Bioenergy Research Center supported by the Office of Biological and Environmental Research in the DOE Office of Science. We are indebted to W. Wang and B. Gu for help with Raman spectroscopy, M. Su and Z. Hu for help with imaging setups, D. B. Geohegan and B. Zhao of ORNL for supplying pluronic coated SWCNHs, and D. Glass for help with animal experiments. We are grateful to V. Castranova at NIOSH for training with the pharyngeal aspiration and BAL techniques. ORNL is managed by UT-Battelle, LLC, for the U.S. Department of Energy under contract DE-AC05-00OR22725.

Author contributions

L.T. and K.T.V. performed the experiments under the guidance of A.P. and T.T. R.M.L. and B.H.V. prepared the samples from the mice. L.T., A.P., K.T.V., B.H.V. and T.T. wrote the manuscript. L.T., A.P. and T.T. carried out revisions of the manuscript. T.T., L.T. and A.P. conceived the experiments. G.S. and V.P.D. helped with the initial assembling of the SNFUH.

Author information

Reprints and permission information is available online at http://npg.nature.com/reprintsandpermissions/. Correspondence and requests for materials should be addressed to A.P.